CHEMISTRY OF MATERIALS

pubs.acs.org/cm

Article

Delamination of Chlorine-Terminated MXene Produced Using Molten Salt Etching

Teng Zhang, Kateryna Shevchuk, Ruocun John Wang, Hyunho Kim, Jamal Hourani, and Yury Gogotsi*

Cite This: *Chem. Mater.* 2024, 36, 1998−2006

Read Online

ACCESS | Metrics & More | Article Recommendations | Supporting Information

ABSTRACT: MXenes produced by Lewis acid molten salt (LAMS) etching of MAX phases have attracted the community's attention due to their controllable surface chemistry. However, their delamination is challenging due to the hydrophobicity of the produced multilayer MXene and strong interactions between the halogen-terminated MXene sheets. The current delamination method involves dangerous chemicals such as *n*-butyllithium or sodium hydride, making scale-up difficult and limiting the practical application of this class of MXenes. In this work, we present a simple and efficient method for the delamination of MXenes from the LAMS synthesis while maintaining their surface chemistry. LiCl salt and anhydrous polar organic solvents are used for delamination. Films produced from the delaminated MXene are flexible and have an electrical conductivity of 8000 S/cm, which is maintained after a week of exposure to 95% humidity. This successful delamination, preservation of inherent surface properties, and stability under high-humidity conditions dramatically expand the range of MXene chemistries available for research and potential applications.

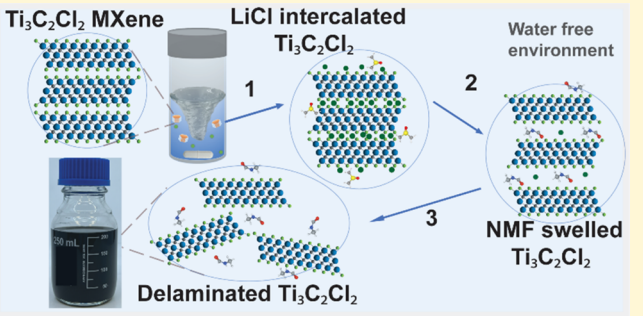

INTRODUCTION

MXenes, a family of two-dimensional (2D) transition metal carbides, carbonitrides, and nitrides, have emerged as versatile materials owing to their unique properties and wide range of potential applications. Since their discovery, the pursuit of effective, efficient, and benign methods for synthesizing and processing MXenes has remained an area of intensive research.[1−6] MXenes are typically produced by the selective etching of layered precursors, such as MAX phases (e.g., Ti_3AlC_2). Among the numerous MXene synthesis methods reported, wet chemical etching in fluorine-containing acids and Lewis acid molten salt (LAMS) etching are currently the only scalable ones. MXenes produced by those methods attract much attention. Acidic etching leads to O/OH-terminated surfaces, eventually with some −F or −Cl.[7−9] These MXenes can be delaminated with an aqueous solution of salts into single-layer flakes for further research, but mixed and oxygen-containing terminations limit the surface chemistry control.[10−12] LAMS synthesis produces MXenes with halogen terminations, offering distinctly different properties and a possibility for substitution with a variety of species and covalent bonding of molecules.[13−16] Nevertheless, delaminating these materials presents significant challenges stemming from the inherent hydrophobic nature of the synthesized MXenes and the robust interlayer interactions among the halogen-terminated MXene sheets. Presently, the delamination has a low yield, and the process relies on using hazardous chemicals, including *n*-butyllithium and sodium hydride (NaH). This complicates the scaling up of production and hinders the broader development and practical deployment of this category of MXenes.[13,17,18] Multiple attempts to delaminate LAMS-MXenes using other methods led to multilayer lamellas rather than high-quality single-layer flakes.[19−22]

To address these challenges, this study presents a safe and straightforward method for the delamination of MXenes synthesized via the LAMS method using LiCl, a benign, abundant, and inexpensive salt, as a delaminating agent. LiCl effectively delaminates MXenes and allows them to retain their surface chemistry, which was a challenging task. Moreover, using LiCl as a delaminating agent ensures the conservation of the intrinsic properties of $Ti_3C_2Cl_2$ MXene, specifically its electrical conductivity of ∼8000 S/cm. Our results demonstrate that this property remains unaltered even under high-humidity conditions, thereby suggesting enhanced environmental stability and widening the scope of MXene applications.

Received: November 10, 2023
Revised: January 16, 2024
Accepted: January 23, 2024
Published: February 6, 2024

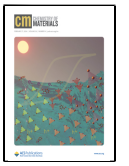

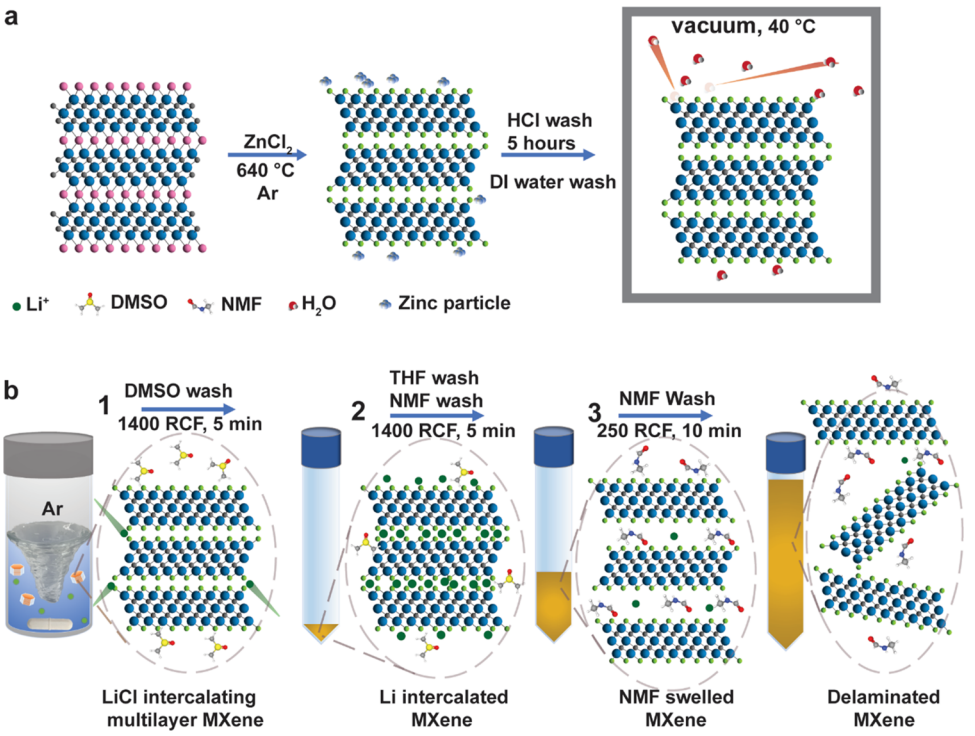

Figure 1. Illustration of (a) Lewis acid molten salt (LAMS) synthesis of uniformly terminated MXene and (b) the delamination process. The delamination is performed under argon.

RESULTS AND DISCUSSION

Synthesis of Multilayer LAMS-MXene. $Ti_3C_2Cl_2$ MXene was synthesized by selective etching of the Al layers from the Ti_3AlC_2 MAX phase precursor using a molten salt etchant with the following reactions:

$$2Ti_3AlC_{2(s)} + 3ZnCl_{2(l)} \rightarrow 2Ti_3C_{2(s)} + 2AlCl_{3(g)} + 3Zn_{(s)} \quad (1)$$

$$2Ti_3C_{2(s)} + 2ZnCl_{2(l)} \rightarrow 2Ti_3C_2Cl_{2(s)} + 2Zn_{(s)} \quad (2)$$

During the reaction, Zn^{2+} is reduced to elemental Zn in the form of molten Zn flux surrounding the multilayer MXene particles, while Al is oxidized to $AlCl_3$ and evaporated as a gas at the reaction temperature of ~660 °C. Elemental Zn melt was mainly evaporated and deposited at the open end of the tube wall, which has a lower temperature. Since oxygen or water is not involved during the reaction, uniform −Cl termination is formed in the synthesized MXene. Once cooled to room temperature, the Zn melt solidified and became nanoparticles and flakes surrounding the multilayer MXene particles. The residual Zn metal in the as-produced $Ti_3C_2Cl_2$ MXene was thoroughly washed away with 12 M HCl. Detailed procedures are shown in the Experimental Section.

Intercalation of LAMS-MXene. We determined that Cl-terminated MXene produced using the LAMS method (Figure 1a) can be delaminated using Li salts in nonaqueous solvents, such as dimethyl sulfoxide (DMSO). Here, we use LiCl as an example (Figure 1b). Since LAMS-MXene is hydrophobic, the hydrated cations are difficult to intercalate between MXene layers. Thus, the whole delamination process must be performed in a moisture-free environment to prevent the hydration shell formation of Li^+. Here, the experiment was performed in an Ar-filled glovebox. First, 1.2 g of LiCl was added to 10 mL of DMSO (Sigma-Aldrich, >99.9%, anhydrous) in a 20 mL glass vial and fully dissolved by stirring with a PTFE-coated magnetic stir bar for 10 min in a closed vial. Then, 3 g of multilayer LAMS-$Ti_3C_2Cl_2$ was added to the solution and stirred at 1000 rpm for 24 h for intercalation. A vortex of MXene was observed.

Swelling of LAMS-MXene. After the treatment with LiCl/DMSO, the Li^+-intercalated multilayer LAMS-$Ti_3C_2Cl_2$ was transferred into a 15 mL centrifuge tube and centrifuged at 1500 RCF for 5 min to remove the DMSO solvent and excess lithium chloride (LiCl, Thermal Scientific Chemicals, anhydrous, 99.0%) salt. To remove the LiCl salt further, 10 mL of tetrahydrofuran (THF, Sigma-Aldrich, anhydrous, ≥99.9%) was added to the tube and washed twice at 1400 RCF for 5 min. After washing with THF and centrifugation, a small volume expansion of MXene sediment was observed compared to DMSO-drained sediment (before THF wash). After removing excess Li^+ cations with THF, the sediment was redispersed into two vials of 15 mL of *N*-methylformamide (NMF, Sigma-Aldrich, >99.9%, anhydrous) for delamination. Heavy swelling was observed with one or two washes with a great volume expansion (~2−3 times), and the MXene had a slurry-like morphology, similar to the delamination process of acid-etched MXene.[11] Therefore, intense manual shaking is required to redisperse the swelled LAMS-MXene into NMF again in this and the following steps for a high yield of delamination. The dark brown supernatant with small multilayers and a few layers of LAMS-MXene was observed during the washing process and decanted into waste. Further washing with NMF resulted in swelling of LAMS-MXene and expansion to ~5 times its original volume, named NMF-swelled MXene (Figures 1b and S1).

When NMF was replaced with *N*-dimethylformamide (DMF, Sigma-Aldrich, anhydrous, 99.8%), a solvent with similar structure and properties, the swelling of MXene was not

https://doi.org/10.1021/acs.chemmater.3c02872
Chem. Mater. 2024, 36, 1998−2006

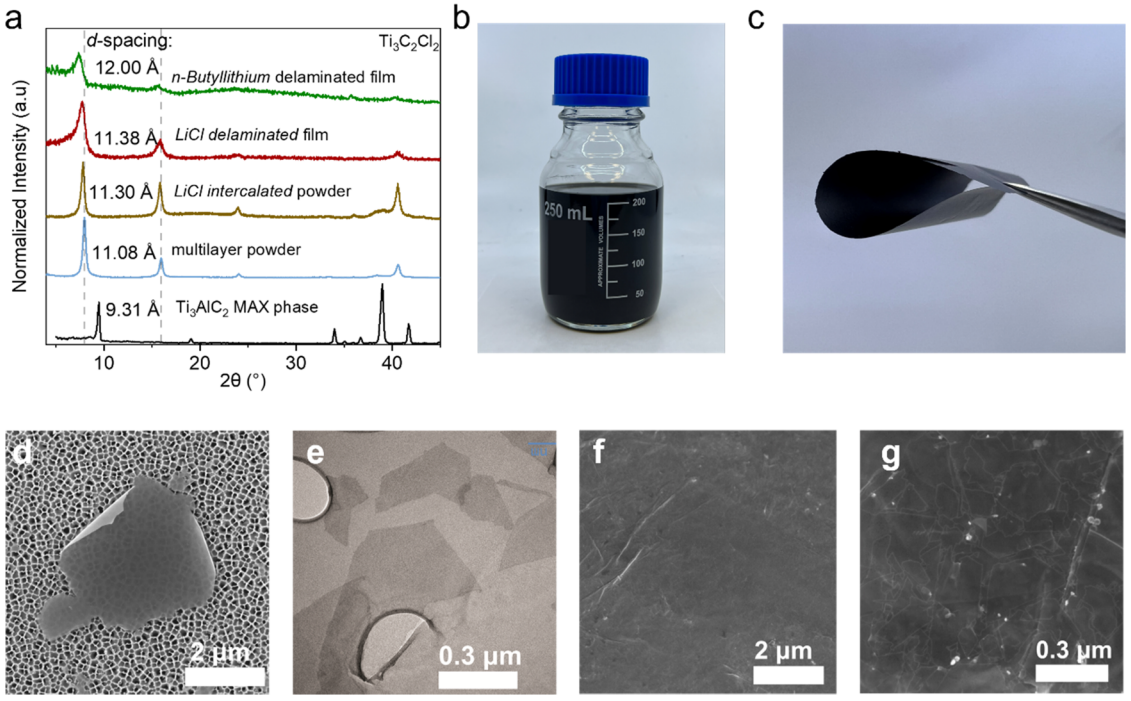

Figure 2. Characterization of LAMS-$Ti_3C_2Cl_2$ MXene. (a) X-ray diffraction patterns of LAMS-$Ti_3C_2Cl_2$ as the pristine multilayer powder (black), LiCl-intercalated multilayer powder (brown), LiCl-delaminated film (red), and *n*-butyllithium-delaminated freestanding film (green). $2\theta = 4$ to 45°. *d*-spacing was calculated based on the (002) peaks. Optical image of (b) LiCl-delaminated LAMS-$Ti_3C_2Cl_2$ solution and (c) the vacuum-filtered freestanding film. (d) Scanning electron microscopy (SEM) and (e) transmission electron microscopy (TEM) images of single-layer $Ti_3C_2Cl_2$ flakes delaminated with LiCl. (f, g) SEM images showing the surface morphology of the LiCl-delaminated LAMS-$Ti_3C_2Cl_2$ freestanding film at different magnifications.

observed after seven washes based on the observation of volume change. One possible explanation could be a significant dielectric constant difference between the two solvents (182 for NMF vs 36.7 for DMF). NMF with a high dielectric constant effectively screens the electrostatic interactions between negatively charged MXene layers and intercalated Li cations and provides better solvation of lithium cations. This weakens the interaction between the MXene layers and aids in the swelling of MXene. Attempts to swell MXene with other polar aprotic solvents, including *N*-methylpyrrolidone (NMP, Sigma-Aldrich, anhydrous, 99.5%), acetonitrile (ACN, Sigma-Aldrich, anhydrous, 99.8%), dimethyl sulfoxide (DMSO, Sigma-Aldrich, >99.9%, anhydrous), and propylene carbonate (PC, Sigma-Aldrich, anhydrous, 99.7%) were unsuccessful (Figure S2).

Delamination of LAMS-MXene in NMF. Continuous washing of NMF-swelled MXene with NMF will result in successful delamination, as noted by observing the dark supernatant after centrifugation at 250 RCF for 5 min. This supernatant contained delaminated MXene with a large flake size and was collected. The collection process was repeated multiple times. The MXene solutions were collected in separate containers for storage. After the supernatant became transparent, the LAMS-MXene sediment was collected and removed from the glovebox. Delamination of LAMS-MXene with *n*-butyllithium was performed as previously reported.[13] We also observed heavy swelling and volume expansion during the delamination process.

To increase the yield of delamination, bath sonication (Branson 2501 Ultrasonic Cleaner, 40 kHz) of residual LAMS-MXene sediment in NMF was performed at room temperature for 20 min in a sealed centrifuge tube under Ar. Then, the solution was delaminated under an ambient environment without argon. The obtained solution was then concentrated by centrifugation at 11,200 RCF for 10 min, and the supernatant was decanted to remove the small flakes of multilayer MXene. The sediment was redispersed with NMF to form an MXene colloidal solution. The MXene solution was stored in a glass bottle and remained stable without aggregation for more than 3 months (Figure S4). The same delamination process was performed using another lithium salt, lithium bis(trifluoromethane)sulfonimide (LiTFSI, TCI, anhydrous, >98.0%). The LAMS-$Ti_3C_2Cl_2$ solution delaminated by LiTFSI was collected for the UV−vis measurement.

Solvent Exchange of Delaminated MXene Solution and Freestanding Film Preparation. LiCl-delaminated LAMS-MXene could be dispersed in other polar solvents, such as DMF, NMP, acetonitrile, DMSO, propylene carbonate, and 2-propanol (IPA, Sigma-Aldrich, anhydrous, 99.5%), by solvent exchange under ambient atmosphere. Considering IPA as an example, NMF-delaminated LAMS-$Ti_3C_2Cl_2$ solution was concentrated with a centrifuge at 11,200 RCF for 10 min. Ten mL of concentrated MXene solution in NMF (~6 mg/mL) was mixed with 30 mL of IPA by manual shaking for 2 min and then centrifuged at 11,200 RCF for 10 min. The clear supernatant was removed, and the MXene sediment was redispersed with an extra 40 mL of IPA and repeated two times. The final sediments were redispersed into IPA and formed a colloidal solution. The solvent-exchange procedure was the same for all of the solvents tested. The colloidal solution stability of LAMS-MXene in protic IPA was much lower than that in polar aprotic solvents such as NMF, DMF, NMP, DMSO, and PC, which were stable for more than 5 days and identified as "good solvents." Sedimentation in IPA was

https://doi.org/10.1021/acs.chemmater.3c02872
Chem. Mater. 2024, 36, 1998−2006

observed after 24 h of storage under ambient conditions (Figure S5). This may come from the low polarity or high hygroscopic nature of IPA, which absorbs water molecules from the ambient atmosphere.

Solvent exchange with other hydroscopic polar solvents with lower dipole moments, including acetone (ACS reagent, ≥99.5%), methanol (anhydrous, 99.8%), and ethanol (200 proof, ACS reagent, ≥99.5%), or with deionized (DI) water failed to produce a colloidal solution. They were identified as "bad solvents" for LAMS-MXene (Figure S5).

Freestanding films of MXene produced by different delamination methods were prepared via vacuum-assisted filtration through a Celgard 3501 membrane.

Direct Delamination of NMF-Swelled MXene in Various Solvents. To address the toxicity concerns associated with NMF, we experimented with alternative, less toxic solvents. This experimentation is detailed in Figures S2 and S3 and the accompanying text, where we demonstrate that successful delamination is universally achievable with NMF-swelled MXene. Our experimental approach involved a two-step process: first swelling the MXene in NMF and then delamination in a different, less toxic aprotic polar solvent. This method was tested with a range of solvents, including DMSO, DMF, NMP, acetonitrile, and PC. Those solvents were employed as the delaminating agents instead of NMF. The delamination protocol followed was similar to that previously described for NMF, as outlined in the "Delamination of LAMS-MXene in NMF" section. The key to this process was using bath sonication for 30 min. This technique enabled us to achieve delamination yields in these alternative solvents comparable to those obtained with NMF. It should be noted that while the procedure has been optimized for NMF, the optimal centrifuge speed and time might differ when using other solvents. Following delamination, the MXene solutions in various solvents were collected and stored in glass vials for further analysis and use. Other delamination routines are discussed in the Supporting Information.

X-ray diffraction (XRD) patterns of the HCl-washed MAX phase and multilayer MXene powder are shown in Figure S7. The elimination of (002), (004), and (104) peaks from the MAX phase confirms the complete conversion from MAX to MXene without zinc peaks in MXene powder, thus indicating the successful removal of zinc metal after the HCl wash.[23,24] The XRD patterns of MXene powder and vacuum-filtered freestanding MXene films are plotted in Figure 2a. Based on the (002) peak position, the *d*-spacing of pristine $Ti_3C_2Cl_2$ MXene is 11.08 Å with a van der Waals (vdW) gap of ∼2.7 Å between MXenes.[13] The *d*-spacing of *n*-butyllithium-delaminated MXene expanded from 11.08 Å of pristine MXene powder to 12.00 Å, which is 0.79 Å larger than that of the reported *n*-butyllithium-treated multilayer powder.[13] Similarly, the *d*-spacing of the LiCl-intercalated MXene powder was 0.22 Å larger than that of the pristine powder, and the corresponding delaminated film had an even greater *d*-spacing (11.38 Å). However, the XRD patterns do not obey Bragg's law. Theoretically, the increase of *d*-spacing at the (002) diffraction pattern is 2 times greater than the (004) diffraction pattern, and visually, the (004) peak should shift farther than the (002) peaks. However, for all three samples, regardless of the intercalated powder or delaminated film, the inverse behavior in XRD patterns is observed: shifts of the (004) patterns are ∼1/2 less than the shift of the (002) patterns. This counterintuitive observation may come from the fact that MXenes are not typical crystals but rather stacks of flakes, which introduces variability in the *d*-spacing measurements.[23,25] The uneven distribution of the layer stacking, flake misalignment, varying flake sizes, the coexistence of few-layered and single-layer MXenes, and confined solvents between the layers result in an unsymmetric peak shape of the (002) peaks in Figure 1a. This indicates that the (002) peak is inaccurate in determining the *d*-spacing. Therefore, the peak position of the (004) pattern was used to determine the *d*-spacing for more accurate results.

Based on the (004) peak position, the *d*-spacing of pristine $Ti_3C_2Cl_2$ MXene is 11.08 Å with a van der Waals (vdW) gap of ∼2.7 Å between MXenes.[13] After delamination with *n*-butyllithium, the *d*-spacing of the MXene freestanding film is 11.36 Å, which is larger than that of *n*-butyllithium treated MXene powder (11.21 Å). The LiCl-intercalated MXene powder and the LiCl-delaminated freestanding film have *d*-spacings of 11.14−11.15 Å. The change of *d*-spacing from intercalated powder to delaminated freestanding films for LiCl MXene was negligible compared to *n*-butyllithium MXene (0.28 Å). This can be explained by the difference in intercalants between the two samples: in *n*-butyllithium-delaminated samples, $Li^+(NMF)_x$ solvents might be confined in MXene layers, whereas only Li^+ ions were confined in LiCl-delaminated MXene layers.[26] One possible explanation could be the difference in intercalants between the two samples: in *n*-butyllithium-delaminated samples, $Li^+(NMF)_x$ solvents may be confined in MXene layers, whereas only Li^+ ions are confined in LiCl-delaminated MXene layers.[26] The LiCl-delaminated film has a higher signal-to-noise ratio (SNR) compared to the *n*-butyllithium-delaminated freestanding film, indicating better flake alignment and more uniform stacking between MXene flakes with the LiCl delamination method. This may help explain the difference in conductivities: the electrical conductivity of *n*-butyllithium-delaminated MXene is ∼2100 S/cm, whereas the LiCl-delaminated film has a conductivity of up to 8000 S/cm, which is comparable with the HF-etched MXene. It is worth noting that both the *n*-butyllithium and NaH were previously reported as highly reactive superbases, which may potentially influence the surface chemistry of MXenes, thus changing the *d*-spacing of delaminated MXene films.

A digital photograph of the collected delaminated MXene solution is shown in Figure 2b. The concentration of MXene can reach 30 mg/mL with a centrifugation process. The vacuum-filtered freestanding film is flexible, and the color is different from previously reported TMAOH-delaminated LAMS-MXene (Figure 2c).[19] Compared to HF-etched MXene, the LAMS-$Ti_3C_2Cl_2$ film is slightly more brittle than the HF-$Ti_3C_2T_x$ film, which may be due to the lack of interlayer water and a hydrogen bond network in the LAMS-$Ti_3C_2Cl_2$ film. The SEM image of single flakes shows LAMS-$Ti_3C_2Cl_2$ that scrolls up at the edge. This is prevalent in the delaminated flakes (Figures 2d and S8a). The TEM image in Figure 2e shows the 2D flake morphology of MXene, indicating successful delamination and separation of single-layer MXene. The cross-sectional SEM image of the LiCl-delaminated LAMS-$Ti_3C_2Cl_2$ freestanding film shows a layered stacked structure (Figure S8b). The surface morphology of the delaminated MXene freestanding film shows a smooth surface across the SEM image (Figure 2f). Interestingly, the high-magnification SEM image shows the MXene flakes stacked underneath other flakes, which has not been observed in HF-

https://doi.org/10.1021/acs.chemmater.3c02872
Chem. Mater. 2024, 36, 1998−2006

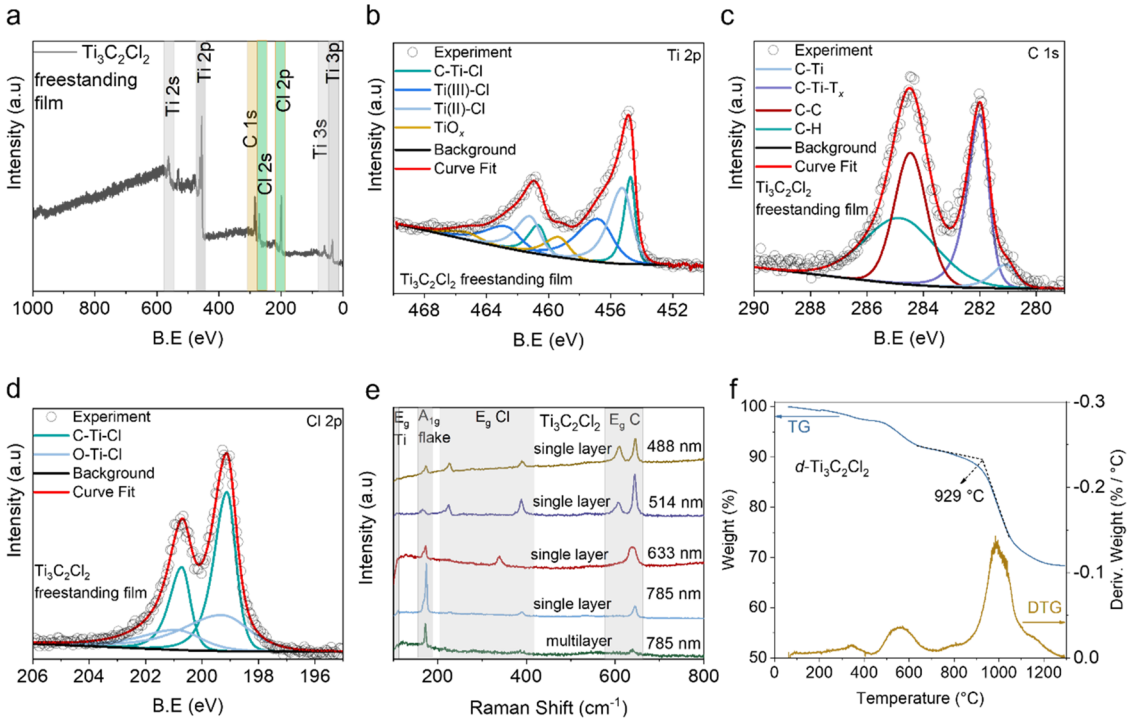

Figure 3. (a–d) XPS spectra of the LiCl-delaminated LAMS-$Ti_3C_2Cl_2$ freestanding film. (a) Survey scan and (b–d) high-resolution XPS spectra of (b) Ti 2p, (c) C 1s, and (d) Cl 2p of the $Ti_3C_2Cl_2$ MXene freestanding film. (e) Raman spectra of LiCl-delaminated LAMS-$Ti_3C_2Cl_2$ MXene on a gold substrate at different laser wavelengths. (f) Thermal gravimetric analysis of the LiCl-delaminated LAMS-$Ti_3C_2Cl_2$ MXene freestanding film.

etched MXene films. This may be due to the absence of confined water between LAMS-$Ti_3C_2Cl_2$ MXene layers and a weaker flake–flake interaction compared to MXenes made via the acid route (due to the absence of hydrogen bonding), resulting in fewer scattering events of secondary electrons across the restacked MXene layers.

The quality of delaminated MXene was examined by survey scan and core-level X-ray photoelectron spectra (XPS, Figures 3a–d and S9). XPS is done without any sputtering to show the actual quality of the MXene film. The survey scan of the LiCl-delaminated MXene freestanding film showed only Ti, C, and Cl peaks and a trivial amount of oxygen, indicating only Cl termination on the surface of the MXene flakes. By fitting the core-level Ti 2p XPS spectrum, the Ti–C component is at 454.7, 455.2, and 456.8 eV, and the trivial Ti–O component is at 459.3 eV, which is attributed to the dissolved oxygen in the X lattice.[27] Strong oxidization of Ti is not observed compared to previously reported delaminated MXene.[19,22] The C 1s spectra show that C–Ti and C–Ti–Cl components have binding energy at 281.1 and 282.0 eV, respectively. The existence of C–C and C–H components in the C 1s spectra comes from the residual NMF solvent and environment. The Cl 2p XPS peaks at 199.1 and 199.3 eV indicate that all Cl are from termination, which bonded with Ti. The O 1s spectra are noisy with low intensity and the majority of the signal comes from C═O/C–O in NMF, indicating the low oxygen content in MXene after the delamination (Figure S10). In general, compared to previously reported delamination of molten salt MXenes, this method shows the cleanest and highest quality in preserving their pristine chemistry to date.

Raman spectra of $Ti_3C_2Cl_2$ MXene provide a comprehensive analysis that elucidates the vibrational characteristics of both multilayer powder and delaminated single flakes, with the latter being probed under four distinct excitation wavelengths: 488, 514, 633, and 785 nm (Figure 3e). For the single-layer flakes, regardless of the excitation wavelength, the consistent presence of the pronounced peak at approximately 600–650 cm^{-1} is evident. This peak can be associated with the out-of-plane vibrations of carbon, an inherent characteristic of MXene M_3X_2 structures. Compared to the $Ti_3C_2T_x$ obtained from the mixed acid etching, this peak has shifted to a lower wavenumber, indicating a softer vibration of the bond affected by Cl surface terminations.[28,29] Moreover, the sharp peaks in the range of 200 to 400 cm^{-1} indicate in-plane and out-of-plane vibrations of the whole flake and surface terminations, suggesting that the material's surface termination is uniform.[30,31] A noteworthy trend is the varying intensity of the primary ∼170 cm^{-1} region and ∼600 cm^{-1} region peaks across the three excitation wavelengths. At 514 nm, the ∼600 cm^{-1} peak exhibits the most pronounced intensity, progressively diminishing with increasing wavelength to 633 nm and subsequently 785 nm. Meanwhile, the ∼170 cm^{-1} peak exhibits the least pronounced intensity at 514 nm, progressively enhancing with increasing wavelength to 633 nm and subsequently 785 nm. For the 488 nm laser wavelength, the 170 cm^{-1} peak is slightly increased, whereas the 600 cm^{-1} peak is decreased compared to the 514 nm wavelength one. For the Raman shift of multilayer MXene powder excited at 785 nm, the peaks at both ∼170 and 600 cm^{-1} are less pronounced than in their single-layer counterparts. This divergence in behavior could be attributed to the complex interlayer interactions and the charges in the interlayer spacing that were observed in HF-etched Ti_3C_2 with increased thickness.[29,31,32]

The thermal stability test of the $Ti_3C_2Cl_2$ MXene freestanding film is performed with thermal gravimetric analysis (Figure 3f). The initial 2.5% weight loss until 400 °C originated from the residual NMF solvent or surface adsorbed water on the sample. As opposed to the HF-etched MXene

https://doi.org/10.1021/acs.chemmater.3c02872
Chem. Mater. 2024, 36, 1998–2006

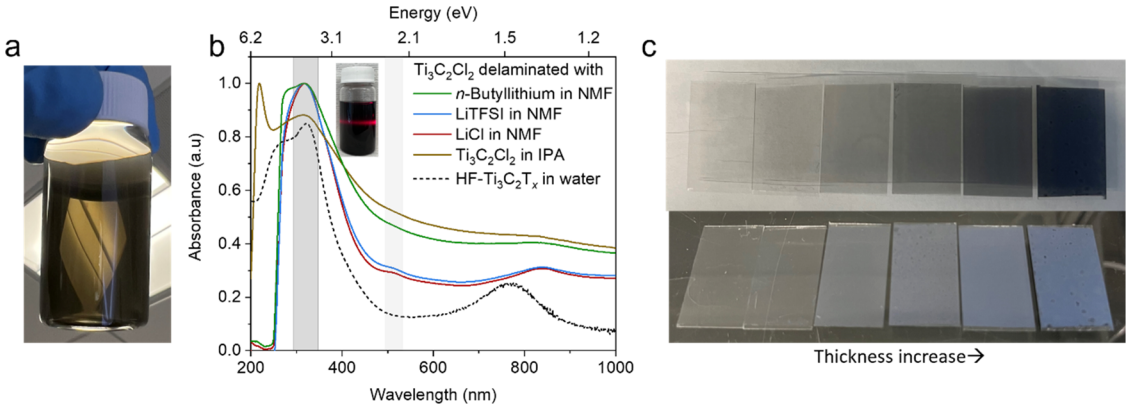

Figure 4. (a) Digital photograph of a $Ti_3C_2Cl_2$ MXene colloidal solution in NMF. (b) UV−vis of $Ti_3C_2Cl_2$ MXene solution with different delamination agents and solvents; the inset picture shows the Tyndall effect. (c) Spray-coated $Ti_3C_2Cl_2$ MXene on a glass substrate with different thicknesses.

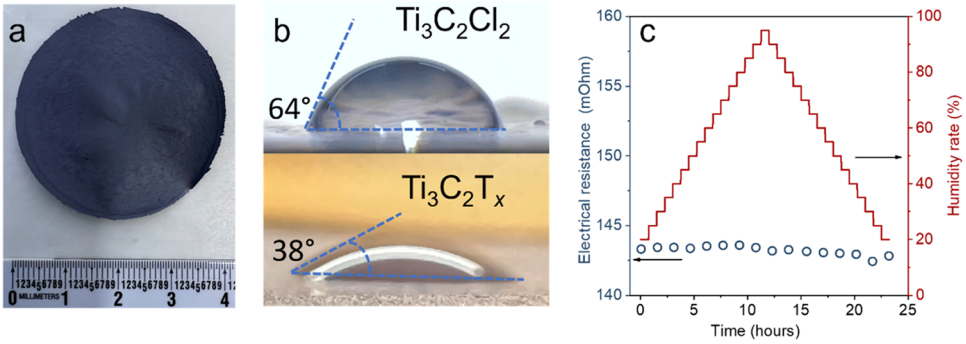

Figure 5. (a) Digital photograph of $Ti_3C_2Cl_2$ MXene freestanding film from the top view. (b) Water contact angles of $Ti_3C_2Cl_2$ MXene freestanding film (top) and HF-etched $Ti_3C_2T_x$ freestanding film. (c) Change of four-point electrical resistance of a $Ti_3C_2Cl_2$ MXene freestanding film between 20 and 95% relative humidity at 35 °C.

film, which decomposed at 800 °C, LAMS-MXene has the second 5.3% weight loss beginning at 480−620 °C, which could be attributed to the loss of Cl termination or formation of vacancies. This process is followed by a 21% weight loss beginning at 929 °C due to the phase transition to cubic titanium carbide (Figures 3f and S11).[14] The thermal decomposition temperature is slightly lower than that of the multilayer $Ti_3C_2Cl_2$ MXene powder; however, the temperature of the structure collapse is 70 °C higher than that of the HF-etched MXene film.[14,33,34]

Different from HF-etched $Ti_3C_2T_x$, whose solution typically has a green color, the $Ti_3C_2Cl_2$ MXene colloidal solution showed a yellowish color regardless of the delamination agent or solvent (Figure 4a). The UV−vis spectra of the MXene solution with all delamination agents showed the absorbance peak at 840 nm, given a 60 nm red shift compared to HF-etched $Ti_3C_2T_x$ because of the different surface terminations. The absorbance peak in the near-infrared (NIR) region of MXene can be assigned to the electronic transitions related to defects, impurities, and functional groups present on the MXene surface.[34,35] MXenes delaminated using the neutral salts LiCl and LiTFSI have a narrower and more pronounced absorbance peak compared to that of *n*-butyllithium-delaminated MXene, suggesting their improved quality (uniformity).[35,36] This may be caused by the superbase nature of *n*-butyllithium, which oxidized the MXene surface and thus broadened the MXene absorbance peak.[35] Regardless of the etching routine, surface chemistry, and solvent, MXene solutions exhibit sharp absorption peaks in the ultraviolet (UV) region at 320 nm, indicating electronic transitions between the valence and conduction bands of the material. This is related to the metallic properties of MXene: the electronic transition occurs at the Ti−C band and is not affected by surface chemistry.[37] Moreover, there is no absorption peak observed in deep UV irradiation, a potentially useful property. Meanwhile, the IPA solution demonstrates a broader absorption peak in this region with a sharp peak near the 200 nm region. The disparity in the shape and intensity of these peaks may suggest differential interactions between the MXene and the solvents, possibly influencing the aggregation state or electronic structure of MXene in these environments, and needs further investigation. Also, a new weak absorption peak was observed at 515 nm, which may reveal a different electronic transition mechanism and needs future exploration with other techniques. The existence of a 515 nm absorbance peak corresponds to the excitation of 514 nm wavelength Raman spectra. The lower wavelength region showed a local minimum absorption of 480 nm. This may explain the suppression of A_{1g} peaks of Raman spectra at ∼600 cm^{-1} for 488 nm wavelength Raman spectra. This change in the absorbance peak strongly correlates with the Raman spectra and needs future investigation. In general, the delaminated MXene with well-controlled terminations opens opportunities for fundamental studies on MXenes with halogen and other terminations.[3,37,38]

https://doi.org/10.1021/acs.chemmater.3c02872
Chem. Mater. 2024, 36, 1998−2006

The MXene in the NMF solution was spray-coated on glass substrates with different thicknesses (Figure 4c). As the thickness of a MXene thin film increases, the decrease of film transmittance is observed on a white background, while the increase of reflection is shown with a black background. A metallic blue color was observed for the spray-coated thin film, as opposed to a purple color that is typical for HF-etched MXene. The termination-induced color change of MXene is attributed to the electronic band structure change with Cl termination.[37,39] The colloidal solution of MXene can be coated on multiple surfaces, making it a good candidate for various practical applications.[40−42]

MXene is known for its hydrophilicity, making it easy to coat on multiple surfaces and giving broader applications such as water deciliation, bioelectronics, electronic ink, wearable electronics, etc.[6] However, the issue arising from the high hydrophilicity is the swelling effect of the MXene film caused by the intercalation of water from the ambient; thus, the hydrolysis induced the instability under a high-humidity environment.[43] A hydrophobic MXene is needed to prevent hydrolysis under a high-humidity environment. One effective solution is the functionalization of pristine MXene with a massive chemical reaction process to introduce hydrophobic molecules on the surface of MXene, which greatly increases the cost and is not practical for real application. Another solution is protonating MXene with hydrochloric acid to create strong layer−layer interaction in the MXene film and prevent the insertion of water molecules. However, this method makes MXene corrosive and nonbiocompatible and may degrade the surface it coated. Knowing that multilayer $Ti_3C_2Cl_2$ MXene is relatively hydrophobic, one would expect its freestanding film to perform similarly. The freestanding film of $Ti_3C_2Cl_2$ MXene showed a smooth surface in both macroscopic and microscopic views (Figures 5a and 2f). The contact angle of water on $Ti_3C_2Cl_2$ MXene is 64°, whereas on HF-etched $Ti_3C_2T_x$ MXene, it is 38°. This is because of the hydrophobic −Cl surface, NMF solvent, and surface microstructure difference in $Ti_3C_2Cl_2$ MXene compared to the HF-etched MXene film (Figure 2g). To test its humidity stability, we measured the in situ electrical resistance in a humidity chamber from 20 to 95 RH%. The humidity stability test of films with an electrical resistance test showed that the conductivity of MXene is not influenced by humidity change, indicating that the water molecules are not intercalated. Also, after storing the film at 95 RH% for 2 weeks, the electrical conductivity of the MXene film remained at 7200 S/cm, which is 90% of its pristine value. Such stable and high-conductivity MXene under high-humidity environments enables its application under complex environments with a lower risk of degradation.

CONCLUSIONS

A safe and high-efficiency protocol for delaminating MXenes synthesized using the LAMS method was developed in this work. We have introduced LiCl in organic solvents as a benign, abundant, inexpensive, and effective delaminating agent. This allowed us to circumvent the challenges traditionally associated with LAMS-MXene delamination, ensuring the preservation of the intrinsic surface chemistry (chlorine terminations) and essential material properties, such as high electronic conductivity. XPS revealed fully preserved halogen terminations after delamination, and lack of oxidation. The delaminated MXene solution showed high colloidal stability for at least 3 months. Distinct optical properties of delaminated LAMS-$Ti_3C_2Cl_2$ are reflected in the Raman and UV−vis spectra due to the change of termination compared to the HF-etched MXenes. The delaminated MXene can be dispersed in IPA, NMF, DMSO, and other polar solvents, spray-coated on a substrate, and processed into a flexible freestanding film. The electrical conductivity of the freestanding film was ∼8000 S/cm, and it was not affected by high humidity. Thermogravimetric analysis showed higher thermal stability compared to the HF-etched $Ti_3C_2T_x$. A universal strategy for the delamination of LAMS-MXene in various polar aprotic solvents has been developed.

EXPERIMENTAL SECTION

Synthesis of the MAX Phase. The MAX phase was synthesized as previously reported.[35] The powder of TiC (Alfa Aesar, 99.5%, 2 μm powder), Ti (Alfa Aesar, 99.5%, 325 mesh), and Al (Alfa Aesar, 99.5%, 325 mesh) were mixed in a molar ratio of 2:1.5:2.2 and mixed with zirconia ball (2:1 mass ratio of precursor powder) for 18 h at a speed of 70 rpm in a HDPE bottle, followed by passivation for 6 h. The mixed powders were transferred into an alumina crucible, followed by annealing in a high-temperature tube furnace (MTI). The tube was maintained with a constant flow of ultra-high-purity Ar at 200 SCCM. The furnace was heated (and cooled) at 3 °C/min to 1380 °C and held for 2 h. The sintered block was then crushed into small pieces and stirred with concentrated HCl (Fisher Scientific, 38 wt %) for 48 h to dissolve away the excess aluminum and intermetallic impurities. Then, the acid-washed MAX phase was washed with deionized water by vacuum-assisted filtration (polycarbonate, pore size <5 μm) until neutral. The MAX phase powder was dried overnight in a vacuum furnace at 80 °C and sieved using a 38 μm sieve for future etching.

LAMS Synthesis of MXene. The LAMS synthesis of MXene was modified from a previously reported method.[13,16,24] A schematic of MXene synthesized by molten salt is shown in Figure 1a. For the synthesis of $Ti_3C_2Cl_2$ MXene, $ZnCl_2$ (Sigma-Aldrich, >99%, anhydrous) was chosen as the Lewis acid. It is hygroscopic and needs to be stored in an Ar- or N_2-filled environment. Therefore, mixing with MAX was performed in an Ar-filled glovebox. First, $ZnCl_2$ was milled into fine powder in a mortar for 10 min. Then, 10 g of Ti_3AlC_2 MAX phase and 80 g of fine $ZnCl_2$ were added into a 250 mL glass bottle and shaken for 2 min for mixing. After mixing the powders, the mix was transferred into an alumina crucible. The filled crucible was then placed in a ziplock bag under argon, transferred out from the glovebox to isolate it from the moisture, and then transferred to a tube furnace (MTI) and heated to 640 °C at 5 °C min^{-1} under constant argon flow (99%, 5 SCCM). The reaction was conducted over 4 h, after which the furnace was cooled at the same rate.

To wash the unreacted $ZnCl_2$ and Zn byproduct, the reacted MS-MXene was transferred out from the tube and added to 200 mL of 12 M HCl in a 500 mL glass bottle. The solution was stirred at 300 rpm for 5 h at room temperature to remove the Zn particles completely. The acid-washed MS-MXene was then transferred into two 125 mL centrifuge vials filled with DI water, washed with a centrifuge at 1400 rcf for 5 min three times. Small MXene flakes pose a problem during filtration because they block the pores of the filter membrane and slow down the filtration process significantly. This step allows the removal of small flakes of MXene beforehand to facilitate the following filtering process. After the centrifuge wash, the multilayer MXene in sediment was redispersed into DI water and filtered by a 5 μm polycarbonate membrane. After the water was dried, more DI water was added. The total volume of DI water for filtering was around 2 L. After filtering, the wet powder was dried in ambient air for 1 h. Then, the powders were transferred into a glass vial and further dried under vacuum at 45 °C for 48 h. The completely dried MXene powders were transferred into the glovebox for future use.

Synthesis of HF-Ti_3C_2. The HF-etched Li−$Ti_3C_2T_x$ was synthesized via a previously reported method.[35]

https://doi.org/10.1021/acs.chemmater.3c02872
Chem. Mater. 2024, 36, 1998−2006

Characterization. X-ray diffraction (XRD) measurements were conducted on the MXene powders and freestanding film by using a Rigaku SmartLab (Tokyo, Japan) diffractometer operating at 40 kV and 30 mA with a Cu Kα X-ray source. The scan range was from 3 to 80° (2θ) with a step scan of 0.02° for 0.6 s holding time. Reflection-mode Raman spectra were collected using a Renishaw InVia Raman microscope (Gloucestershire, U.K.) spectrometer using an ×63 objective and 1800 line/mm grating with 488, 514, 633, and 785 nm laser wavelengths. The MXene flakes and powders were deposited on a gold-coated glass substrate. Scanning electron microscopy (SEM) analysis was performed using a Zeiss Supra 50VP microscope with a 3 kV beam, 5 mm working distance, and in-lens detector. XPS spectra were collected on a PHI VersaProbe 5000 instrument (Physical Electronics) spectrometer by using a 200 μm and 50 W monochromatic Al Kα X-ray source (1486.6 eV) and a 23.5 eV pass energy with a step size of 0.05 eV. The MXene freestanding film is loaded on conductive carbon tapes without sputtering. Peak fitting of high-resolution XPS spectra was performed with CasaXPS V2.3.25 software. A Tougaard background was used for transition-metal-based compounds. An in situ resistance−humidity test was performed using the Memmert HCP50 humidity chamber and a four-point probe connected with the Keithley 2400 SourceMeter. The humidity chamber was set at a 20 − 95 − 20% humidity rate with a step size of 5 HR% at 35 °C. Each humidity was held for 45 min for stabilizing humidity. The resistance was recorded with the Keithley Kickstart software.

■ ASSOCIATED CONTENT

Supporting Information

The Supporting Information is available free of charge at https://pubs.acs.org/doi/10.1021/acs.chemmater.3c02872.

Additional X-ray diffraction patterns; scanning electron micrographs; X-ray photoelectron spectra; thermal gravimetric analysis data; optical photos of MXene solution; flowchart of delamination, and a detailed discussion of the different routines (PDF)

■ AUTHOR INFORMATION

Corresponding Author

Yury Gogotsi − *A.J. Drexel Nanomaterials Institute and Department of Materials Science and Engineering, Drexel University, Philadelphia, Pennsylvania 19104, United States;* orcid.org/0000-0001-9423-4032; Email: gogotsi@drexel.edu

Authors

Teng Zhang − *A.J. Drexel Nanomaterials Institute and Department of Materials Science and Engineering, Drexel University, Philadelphia, Pennsylvania 19104, United States;* orcid.org/0000-0002-4939-0594

Kateryna Shevchuk − *A.J. Drexel Nanomaterials Institute and Department of Materials Science and Engineering, Drexel University, Philadelphia, Pennsylvania 19104, United States;* orcid.org/0000-0001-7411-3110

Ruocun John Wang − *A.J. Drexel Nanomaterials Institute and Department of Materials Science and Engineering, Drexel University, Philadelphia, Pennsylvania 19104, United States;* orcid.org/0000-0001-8095-5285

Hyunho Kim − *A.J. Drexel Nanomaterials Institute and Department of Materials Science and Engineering, Drexel University, Philadelphia, Pennsylvania 19104, United States;* orcid.org/0000-0003-2381-9716

Jamal Hourani − *A.J. Drexel Nanomaterials Institute and Department of Materials Science and Engineering, Drexel University, Philadelphia, Pennsylvania 19104, United States*

Complete contact information is available at: https://pubs.acs.org/10.1021/acs.chemmater.3c02872

Author Contributions

T.Z. conducted the synthesis and performed the XRD, XPS, SEM, and optical and electrical conductivity characterization. K.S. performed the Raman characterization. R.W. performed the humidity analysis. H.K. assisted in interpreting optical and Raman results. J.H. performed the thin-film fabrication. Y.G. supervised the project. The manuscript was written through contributions of all authors. All authors have approved the final version of the manuscript.

Notes

The authors declare no competing financial interest.

■ ACKNOWLEDGMENTS

This work was supported by the U.S. Department of Energy (DOE), Office of Science, Office of Basic Energy Sciences, Grant No. DE-SC0018618, and the U.S. National Science Foundation under Grant Number CHE-2318105 (M-STAR CCI). Any opinions, findings, conclusions, or recommendations expressed in this material are those of the author(s) and do not necessarily reflect the views of the U.S. Department of Energy or the U.S. National Science Foundation. The authors thank Robert Lord for helping with TEM imaging and Drexel Material Characterization Core (MCC) for providing access to SEM, XPS, TEM, and XRD characterization tools.

■ REFERENCES

(1) Naguib, M.; Kurtoglu, M.; Presser, V.; Lu, J.; Niu, J.; Heon, M.; Hultman, L.; Gogotsi, Y.; Barsoum, M. W. Two-Dimensional Nanocrystals Produced by Exfoliation of Ti_3AlC_2. *Adv. Mater.* **2011**, *23* (37), 4248−4253.

(2) Li, X.; Huang, Z.; Shuck, C. E.; Liang, G.; Gogotsi, Y.; Zhi, C. MXene Chemistry, Electrochemistry and Energy Storage Applications. *Nat. Rev. Chem.* **2022**, *6*, 389−404.

(3) Anasori, B.; Gogotsi, Y. MXenes: Trends, Growth, and Future Directions. *Graphene 2D Mater.* **2022**, *7* (3−4), 75−79.

(4) Gogotsi, Y.; Anasori, B. The Rise of MXenes. *ACS Nano* **2019**, *13* (8), 8491−8494.

(5) Lim, K. R. G.; Shekhirev, M.; Wyatt, B. C.; Anasori, B.; Gogotsi, Y.; Seh, Z. W. Fundamentals of MXene Synthesis. *Nat. Synth.* **2022**, *1* (8), 601−614.

(6) VahidMohammadi, A.; Rosen, J.; Gogotsi, Y. The world of two-dimensional carbides and nitrides (MXenes). *Science* **2021**, *372*, No. eabf1581.

(7) Natu, V.; Barsoum, M. W. MXene Surface Terminations: A Perspective. *J. Phys. Chem. C* **2023**, *127* (41), 20197−20206.

(8) Anayee, M.; Shuck, C. E.; Shekhirev, M.; Goad, A.; Wang, R.; Gogotsi, Y. Kinetics of Ti_3AlC_2 Etching for $Ti_3C_2T_x$ MXene Synthesis. *Chem. Mater.* **2022**, *34* (21), 9589−9600.

(9) Griffith, K. J.; Hope, M. A.; Reeves, P. J.; Anayee, M.; Gogotsi, Y.; Grey, C. P. Bulk and Surface Chemistry of the Niobium MAX and MXene Phases from Multinuclear Solid-State NMR Spectroscopy. *J. Am. Chem. Soc.* **2020**, *142* (44), 18924−18935.

(10) Mashtalir, O.; Naguib, M.; Mochalin, V. N.; Dall'Agnese, Y.; Heon, M.; Barsoum, M. W.; Gogotsi, Y. Intercalation and Delamination of Layered Carbides and Carbonitrides. *Nat. Commun.* **2013**, *4* (1), No. 1716.

(11) Alhabeb, M.; Maleski, K.; Anasori, B.; Lelyukh, P.; Clark, L.; Sin, S.; Gogotsi, Y. Guidelines for Synthesis and Processing of Two-Dimensional Titanium Carbide ($Ti_3C_2T_x$ MXene). *Chem. Mater.* **2017**, *29* (18), 7633−7644.

(12) Hart, J. L.; Hantanasirisakul, K.; Lang, A. C.; Anasori, B.; Pinto, D.; Pivak, Y.; van Omme, J. T.; May, S. J.; Gogotsi, Y.; Taheri, M. L.

Control of MXenes' Electronic Properties through Termination and Intercalation. *Nat. Commun.* **2019**, *10* (1), No. 522.
(13) Kamysbayev, V.; Filatov, A. S.; Hu, H.; Rui, X.; Lagunas, F.; Wang, D.; Klie, R. F.; Talapin, D. V. Covalent Surface Modifications and Superconductivity of Two-Dimensional Metal Carbide MXenes. *Science* **2020**, *369* (6506), 979−983.
(14) Li, Y.; Shao, H.; Lin, Z.; Lu, J.; Liu, L.; Duployer, B.; Persson, P. O. Å.; Eklund, P.; Hultman, L.; Li, M.; Chen, K.; Zha, X.-H.; Du, S.; Rozier, P.; Chai, Z.; Raymundo-Piñero, E.; Taberna, P.-L.; Simon, P.; Huang, Q. A General Lewis Acidic Etching Route for Preparing MXenes with Enhanced Electrochemical Performance in Non-Aqueous Electrolyte. *Nat. Mater.* **2020**, *19* (8), 894−899.
(15) Li, M.; Li, X.; Qin, G.; Luo, K.; Lu, J.; Li, Y.; Liang, G.; Huang, Z.; Zhou, J.; Hultman, L.; Eklund, P.; Persson, P. O. Å.; Du, S.; Chai, Z.; Zhi, C.; Huang, Q. Halogenated Ti_3C_2 MXenes with Electrochemically Active Terminals for High-Performance Zinc Ion Batteries. *ACS Nano* **2021**, *15* (1), 1077−1085.
(16) Ding, H.; Li, Y.; Li, M.; Chen, K.; Liang, K.; Chen, G.; Lu, J.; Palisaitis, J.; Persson, O. Å.; Eklund, P.; Hultman, L.; Du, S.; Chai, Z.; Gogotsi, Y.; Huang, Q. Chemical Scissor-Mediated Structural Editing of Layered Transition Metal Carbides. *Science* **2023**, *379* (6637), 1130−1135.
(17) Wang, D.; Zhou, C.; Filatov, A. S.; Cho, W.; Lagunas, F.; Wang, M.; Vaikuntanathan, S.; Liu, C.; Klie, R. F.; Talapin, D. V. Direct Synthesis and Chemical Vapor Deposition of 2D Carbide and Nitride MXenes. *Science* **2023**, *379* (6638), 1242−1247.
(18) Zhou, C.; Wang, D.; Lagunas, F.; Atterberry, B.; Lei, M.; Hu, H.; Zhou, Z.; Filatov, A. S.; Jiang, D.-e.; Rossini, A. J.; Klie, R. F.; Talapin, D. V. Hybrid Organic−Inorganic Two-Dimensional Metal Carbide MXenes with Amido- and Imido-Terminated Surfaces. *Nat. Chem.* **2023**, *15* (12), 1722−1729.
(19) Liu, L.; Orbay, M.; Luo, S.; Duluard, S.; Shao, H.; Harmel, J.; Rozier, P.; Taberna, P.-L.; Simon, P. Exfoliation and Delamination of $Ti_3C_2T_x$ MXene Prepared *via* Molten Salt Etching Route. *ACS Nano* **2022**, *16* (1), 111−118.
(20) Arole, K.; Blivin, J. W.; Bruce, A. M.; Athavale, S.; Echols, I. J.; Cao, H.; Tan, Z.; Radovic, M.; Lutkenhaus, J. L.; Green, M. J. Exfoliation, Delamination, and Oxidation Stability of Molten Salt Etched Nb_2CT_z MXene Nanosheets. *Chem. Commun.* **2022**, *58* (73), 10202−10205.
(21) Arole, K.; Blivin, J. W.; Saha, S.; Holta, D. E.; Zhao, X.; Sarmah, A.; Cao, H.; Radovic, M.; Lutkenhaus, J. L.; Green, M. J. Water-Dispersible $Ti_3C_2T_z$ MXene Nanosheets by Molten Salt Etching. *iScience* **2021**, *24* (12), No. 103403.
(22) Wang, X.; Shi, Y.; Qiu, J.; Wang, Z. Molten-Salt Etching Synthesis of Delaminatable MXenes. *Chem. Commun.* **2023**, *59* (34), 5063−5066.
(23) Shekhirev, M.; Shuck, C. E.; Sarycheva, A.; Gogotsi, Y. Characterization of MXenes at Every Step, from Their Precursors to Single Flakes and Assembled Films. *Prog. Mater. Sci.* **2021**, *120*, No. 100757.
(24) Li, M.; Lu, J.; Luo, K.; Li, Y.; Chang, K.; Chen, K.; Zhou, J.; Rosen, J.; Hultman, L.; Eklund, P.; O Å Persson, P.; Du, S.; Chai, Z.; Huang, Z.; Huang, Q. Element Replacement Approach by Reaction with Lewis Acidic Molten Salts to Synthesize Nanolaminated MAX Phases and MXenes. *J. Am. Chem. Soc.* **2019**, *141* (11), 4730−4737.
(25) Célérier, S.; Hurand, S.; Garnero, C.; Morisset, S.; Benchakar, M.; Habrioux, A.; Chartier, P.; Mauchamp, V.; Findling, N.; Lanson, B.; Ferrage, E. Hydration of $Ti_3C_2T_x$ MXene: An Interstratification Process with Major Implications on Physical Properties. *Chem. Mater.* **2019**, *31* (2), 454−461.
(26) Wang, X.; Mathis, T. S.; Li, K.; Lin, Z.; Vlcek, L.; Torita, T.; Osti, N. C.; Hatter, C.; Urbankowski, P.; Sarycheva, A.; Tyagi, M.; Mamontov, E.; Simon, P.; Gogotsi, Y. Influences from Solvents on Charge Storage in Titanium Carbide MXenes. *Nat. Energy* **2019**, *4* (3), 241−248.
(27) Michałowski, P. P.; Anayee, M.; Mathis, T. S.; Kozdra, S.; Wójcik, A.; Hantanasirisakul, K.; Jóźwik, I.; Piątkowska, A.; Możdżonek, M.; Malinowska, A.; Diduszko, R.; Wierzbicka, E.; Gogotsi, Y. Oxycarbide MXenes and MAX Phases Identification Using Monoatomic Layer-by-Layer Analysis with Ultralow-Energy Secondary-Ion Mass Spectrometry. *Nat. Nanotechnol.* **2022**, *17* (11), 1192−1197.
(28) Shevchuk, K.; Sarycheva, A.; Shuck, C. E.; Gogotsi, Y. Raman Spectroscopy Characterization of 2D Carbide and Carbonitride MXenes. *Chem. Mater.* **2023**, *35* (19), 8239−8247.
(29) Sarycheva, A.; Gogotsi, Y. Raman Spectroscopy Analysis of the Structure and Surface Chemistry of $Ti_3C_2T_x$ MXene. *Chem. Mater.* **2020**, *32* (8), 3480−3488.
(30) Hu, T.; Wang, J.; Zhang, H.; Li, Z.; Hu, M.; Wang, X. Vibrational Properties of Ti_3C_2 and $Ti_3C_2T_2$ (T = O, F, OH) Monosheets by First-Principles Calculations: A Comparative Study. *Phys. Chem. Chem. Phys.* **2015**, *17* (15), 9997−10003.
(31) Berger, E.; Lv, Z.-P.; Komsa, H.-P. Raman Spectra of 2D Titanium Carbide MXene from Machine-Learning Force Field Molecular Dynamics. *J. Mater. Chem. C* **2023**, *11* (4), 1311−1319.
(32) Gouadec, G.; Colomban, P. Raman Spectroscopy of Nanomaterials: How Spectra Relate to Disorder, Particle Size and Mechanical Properties. *Prog. Cryst. Growth Charact. Mater.* **2007**, *53* (1), 1−56.
(33) Seredych, M.; Shuck, C. E.; Pinto, D.; Alhabeb, M.; Precetti, E.; Deysher, G.; Anasori, B.; Kurra, N.; Gogotsi, Y. High-Temperature Behavior and Surface Chemistry of Carbide MXenes Studied by Thermal Analysis. *Chem. Mater.* **2019**, *31* (9), 3324−3332.
(34) Zhang, T.; Shuck, C. E.; Shevchuk, K.; Anayee, M.; Gogotsi, Y. Synthesis of Three Families of Titanium Carbonitride MXenes. *J. Am. Chem. Soc.* **2023**, *145* (41), 22374−22383.
(35) Mathis, T. S.; Maleski, K.; Goad, A.; Sarycheva, A.; Anayee, M.; Foucher, A. C.; Hantanasirisakul, K.; Shuck, C. E.; Stach, E. A.; Gogotsi, Y. Modified MAX Phase Synthesis for Environmentally Stable and Highly Conductive Ti_3C_2 MXene. *ACS Nano* **2021**, *15* (4), 6420−6429.
(36) Hantanasirisakul, K.; Alhabeb, M.; Lipatov, A.; Maleski, K.; Anasori, B.; Salles, P.; Ieosakulrat, C.; Pakawatpanurut, P.; Sinitskii, A.; May, S. J.; Gogotsi, Y. Effects of Synthesis and Processing on Optoelectronic Properties of Titanium Carbonitride MXene. *Chem. Mater.* **2019**, *31* (8), 2941−2951.
(37) Hantanasirisakul, K.; Gogotsi, Y. Electronic and Optical Properties of 2D Transition Metal Carbides and Nitrides (MXenes). *Adv. Mater.* **2018**, *30* (52), No. 1804779.
(38) Gogotsi, Y.; Huang, Q. MXenes: Two-Dimensional Building Blocks for Future Materials and Devices. *ACS Nano* **2021**, *15* (4), 5775−5780.
(39) Azadi, S. K.; Zeynali, M.; Asgharizadeh, S.; Fooladloo, M. A. Investigation of the Optical and Electronic Properties of Functionalized Ti_3C_2 Mxene with Halid Atoms Using DFT Calculation. *Mater. Today Commun.* **2023**, *35*, No. 106136.
(40) Shahzad, F.; Alhabeb, M.; Hatter, C. B.; Anasori, B.; Hong, S. M.; Koo, C. M.; Gogotsi, Y. Electromagnetic Interference Shielding with 2D Transition Metal Carbides (MXenes). *Science* **2016**, *353* (6304), 1137−1140.
(41) Simon, P.; Gogotsi, Y. Perspectives for Electrochemical Capacitors and Related Devices. *Nat. Mater.* **2020**, *19* (11), 1151−1163.
(42) Cai, Y.; Shen, J.; Yang, C. W.; Wan, Y.; Tang, H. L.; Aljarb, A. A.; Chen, C.; Fu, J. H.; Wei, X.; Huang, K. W.; Han, Y.; Jonas, S. J.; Dong, X.; Tung, V. Mixed-Dimensional MXene-Hydrogel Heterostructures for Electronic Skin Sensors with Ultrabroad Working Range. *Sci. Adv.* **2020**, *6* (48), No. eabb5367.
(43) Zaman, W.; Matsumoto, R. A.; Thompson, M. W.; Liu, Y.-H.; Bootwala, Y.; Dixit, M. B.; Nemsak, S.; Crumlin, E.; Hatzell, M. C.; Cummings, P. T.; Hatzell, K. B. In Situ Investigation of Water on MXene Interfaces. *Proc. Natl. Acad. Sci. U.S.A.* **2021**, *118* (49), No. e2108325118.

https://doi.org/10.1021/acs.chemmater.3c02872
Chem. Mater. 2024, 36, 1998−2006